

Contents lists available at ScienceDirect

Applied Mathematics and Computation

journal homepage: www.elsevier.com/locate/amc



NURBS curves with the application of multiple bones fracture reconstruction



Abdul Majeed a.*, Abd Rahni Mt Piah b, Muhammad Rafique c, Johari Yap Abdullah^d, Zainul Ahmad Rajion^d

- ^a Division of Science and Technology, University of Education Town Ship Lahore, Pakistan
- ^b School of Mathematical Sciences, Universiti Sains Malaysia, USM Pulau Penang 11800, Malaysia
- ^c National University of Science and Technology, Islamabad, Pakistan
- ^d Craniofacial Medical Imaging Research Group, School of Dental Sciences, Universiti Sains Malaysia, Kota Bharu 16150, Kelantan, Malaysia

ARTICLE INFO

Keywords: CT scan DICOM data Boundary extraction Chord length parametrization NURBS curves Multiple bones fracture reconstruction

ABSTRACT

The challenging task of treating trauma to cranio-maxillofacial requires advanced radiological imaging and high clinical skills. The reconstruction of facial fractures focuses on the rehabilitation of patients functionally as well as in aesthetics. In this article we used NURBS curves to construct the multiple bones fracture using CT scan data in Digital Imaging and Communications in Medicine (DICOM) format. The reconstruction process of multiple bones fracture start with the boundary extraction followed by corner detection, optimization of knots, weights, construction of fractured part inner outer curve for each CT scan slice using NURBS curves and finally the construction of fractured part in DICOM format. The construction process using proposed method is based on DICOM data only that does not require any technique such as technical help, mirror imaging, to take average thickness of skull bone or reference skull, etc. The constructed fractured implant is custom made for each patient. We present a real case in which multiple bones fracture has been constructed using NURBS curves. The proposed method has also been validated quantitatively and qualitatively using self supposed fractured data.

© 2017 Elsevier Inc. All rights reserved.

1. Introduction

The complicated cranio-maxillofacial region resides various vital viscera. The etiological factors such as road traffic accidents, sports injury, tumors and congenital anomalies attribute to disruption of normal anatomical profile of this region. Fig. 1 shows the inter linkages of different bones of this region. The deformation in the craniofacial region does not follow any specific pattern. The fractures in craniofacial region are diagnosed through different imaging technologies such as CT scan and MRI.

CAD/CAM is extensively used for reconstruction of fractured segments of craniofacial region [1,2] but this technique is expensive and requires advanced skills and practical experience. Other methods propose the solution without CAD processing but have their own limitations such as mirroring method [3] that works in unilateral fracture only and reference model method [4] that is not customized solution for individual patient, Hughes et al. [5] have constructed the exact geometric

E-mail address: abdulmajeed@ue.edu.pk (A. Majeed).

^{*} Corresponding author.

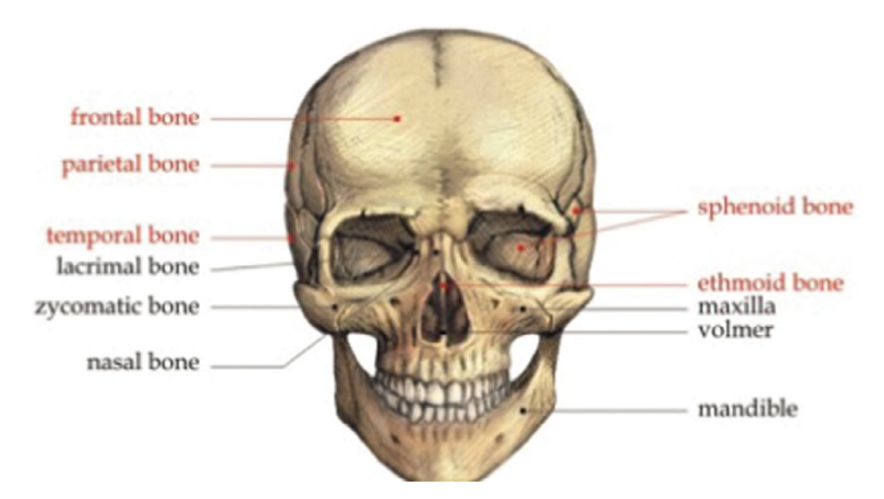


Fig. 1. Craniofacial bones.

model using the NURBS (Non-Uniform Rational B-Spline) basis functions. The use of this model is to analyze, refine the basis or to elevate the order of basis without changing the geometry or its parametrization. Nguyen-Thanh et al. [6] have suggested an alternative approach based on polynomial splines to NURBS-based Isogeometric analysis that is also applicable for local renement and exploits the flexibility of T-meshes for local renement. Isogeothermic analysis of thin shells using polynomial splines over hierarchical T-meshes (PHT-splines) is proposed by Nguyen-Thanh et al. [7]. An alternative approach to the standard finite element heterogeneous multi-scale method (FE-HMM) in form of Isogeometric analysis heterogeneous multiscale method (IGA-HMM) using Non-Uniform Rational B-Splines (NURBS) is suggested in [8]. Yin et al. [9] have used non-uniform rational basis functions for critical buckling parameters and natural frequencies of defective functionally graded material (FGM). Carr et al. [10] used radial basis function (RBF) in reconstruction of facial defects. Carr et al. [11] have incorporated the radial basis function in construction of 3D objects and Chowdhury et al. [12] managed the virtual reconstruction of mandible bone fracture by using iterative closest point (ICP) and taking non-fractured bone contour as reference contour. GC^1 rational Ball curve has been used in [13] for the reconstruction of parietal bone fracture part.

Bui et al. [14] have used the NURBS basis functions for the development of dynamic extended isogeometric analysis (XIGA) for transient fracture of cracked magneto electro elastic (MEE) solids under coupled electro-magneto-mechanical loading. Yu et al. [15] have investigated the thermal buckling behaviors of FGPs with internal defects like cutouts or cracks using NURBS based XIGA with level sets and the FSDT. Bui et al. [16] have used NURBS basis functions to develop dynamic model based on the XIGA. Non-Uniform Rational B-Spline (NURBS) basis functions have been used in [17] to generate accurate and effective scheme for simulating free vibrations and buckling problems of laminated composite plates with cutouts. For more work (see [18–22], and references therein).

This article presents the multiple bones fracture reconstruction using NURBS curves. The process of reconstruction starts by checking the applicability of proposed method by reconstructing the boundary curve of complete CT scan image. Mathematical morphology is used to obtain the boundary of complete CT scan image. Proposed method is then used to reconstruct the boundary curves of traumatized part of all CT scan slices. The boundary curves can be changed or adjusted by weights. On getting the satisfactory boundary curves, the fractured parts are converted to DICOM format using the boundary curves. The suggested method is time efficient, custom made implant for every individual patient and user friendly since there is no need to take mirror image, to construct the reference model, technical help and to take the average thickness of skull bone.

The suggested method has been validated by reconstructing self supposed parietal bone fractured part which gives the same result and overlap with the original. Case report of multiple bones fracture has been presented to show the applicability and validity of proposed method. The DICOM data are obtained from Hospital Universiti Sains Malaysia (HUSM). We employ MATLAB for the programming. The fractured part can be changed or adjusted by changing the position of knot points.

1.1. Objectives and significance of study

The objectives of this study are

- To provide the method for the construction of multiple bones fracture.
- To apply NURBS curves for the construction of inner and outer curves of fractured part and construct the fractured part into DICOM format.
 - To provide the initial platform of custom-made implant for every patient with craniofacial fractures.

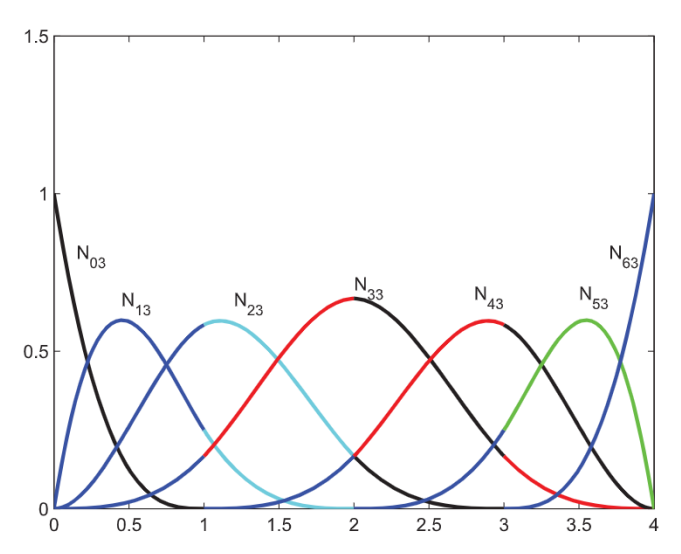


Fig. 2. B-spline basis with non-uniform knots.

This study is significant because

- It provide the methods to attain the required thickness of bone.
- It provide the custom made implant for every unique patient.
- It provide the best solution or treatment option for the benefit of the patient.

2. Theoretical foundation

This section explains the mathematics involved for the construction of multiple bones fracture.

2.1. The Non-Uniform Rational B Spline (NURBS) curves

A dth-degree NURBS curve is defined by

$$S(t) = \frac{\sum_{i=0}^{n} N_{i,d}(t) w_i P_i}{\sum_{i=0}^{n} N_{i,d}(t) w_i}, \ a \le t \le b.$$
 (1)

where $\{P_i\}$ are the control points $\{w_i\}$ are the weights and $\{N_{i,d}(t)\}$ are the dth-degree B spline basis functions defined on the non-uniform knot vector

$$T = \{\underbrace{a, \ldots a}_{d+1}, t_{d+1}, \ldots, t_{m-p-1}, \underbrace{b, \ldots, b}_{d+1}\}.$$

as

$$N_{i,0}(t) = \begin{cases} 1, & \text{if } t \in [t_i, t_{i+1}), \\ 0, & \text{otherwise.} \end{cases}$$
 (2)

$$N_{i,d}(t) = \frac{t - t_i}{t_{i+d} - t_i} N_{i,d-1}(t) + \frac{t_{i+d+1} - t}{t_{i+d+1} - t_{i+1}} N_{i+1,d-1}(t)$$
(3)

for i = 0, ..., n and $d \ge 1$.

For simplicity, we assume that a = 0, b = 1, and $w_i > 0$ for all i. Setting

$$R_{i,d}(t) = \frac{N_{i,d}(t)w_i}{\sum_{j=0}^{n} N_{i,d}(t)w_j},$$
(4)

Eq. (1) can be written as

$$S(t) = \sum_{i=0}^{n} R_{i,d}(t) P_i.$$
 (5)

The $R_{i,d}(t)$ are the rational basis functions. Fig. 2 shows the graphical behavior of basis. These basis are piecewise rational functions on $t \in [0, 1]$.

The NURBS curves S(t) as defined in Eq. (5) have the following properties:

- $S(0) = P_0$ and $S(1) = P_n$;
- $R_{0,d}(0) = R_{N,d}(1) = 1$.
- For $d \ge 0$, all $R_{i,d}(t)$ attain exactly one maximum on the interval $t \in [0, 1]$.
- Local support: $R_{i,d}(t) = 0$ for $t \notin [t_i, t_{i+1}]$. Furthermore, in any given knot span, at most d+1 of the $R_{i,d}(t)$ are nonzero.
- If $w_i = 1 \ \forall i$, then $R_{i,d}(t) = N_{i,d}(t)$ for all i i.e., the $N_{i,d}(t)$ are special case of the $R_{i,d}(t)$.

2.2. Cubic NURBS curves

$$T = \{\underbrace{0, \dots 0}_{4}, t_{5}, \dots, t_{m-p-1}, \underbrace{1, \dots, 1}_{4} \} \text{ are }$$

$$d = 1$$

$$N_{i,0}(t) = \begin{cases} 1, & \text{if } t \in [t_{i}, t_{i+1}), \\ 0, & \text{otherwise.} \end{cases}$$

$$d = 1$$

$$N_{2,1}(t) = \frac{t_4 - t}{t_4 - t_3} N_{3,0}(t),$$

$$N_{j,1}(t) = \frac{t - t_j}{t_{j+1} - t_j} N_{j,0}(t) + \frac{t_{j+2} - t}{t_{j+2} - t_{j+1}} N_{j+1,0}(t), \quad 3 \le j \le m - 5$$

$$N_{m-4,1}(t) = \frac{t - t_{m-4}}{t_{m-3} - t_{m-4}} N_{m-4,0}(t).$$

$$d = 2$$

$$N_{1,2}(t) = \frac{(t_4 - t)(t_4 - t)}{(t_4 - t_3)(t_4 - t_2)} N_{3,0}(t),$$

$$N_{2,2}(t) = \left[\frac{(t-t_2)(t_4-t)}{(t_4-t_3)(t_4-t_2)} + \frac{(t_5-t)(t-t_3)}{(t_5-t_3)(t_4-t_3)} \right] N_{3,0}(t) + \frac{(t_5-t)^2}{(t_5-t_3)(t_5-t_4)} N_{4,0}(t),$$

$$\begin{split} N_{j,2}(t) &= \frac{(t-t_j)^2}{(t_{j+1}-t_j)(t_{j+2}-t_j)} N_{j,0}(t) + \cdots \\ & \left[\frac{(t-t_j)(t_{j+2}-t)}{(t_{j+2}-t_j)(t_{j+2}-t_{j+1})} + \frac{(t_{j+3}-t)(t-t_{j+1})}{(t_{j+3}-t_{j+1})(t_{j+2}-t_{j+1})} \right] N_{j+1,0}(t) + \cdots \\ & \frac{(t_{j+3}-t)^2}{(t_{j+3}-t_{j+1})(t_{j+3}-t_{j+2})} N_{j+2,0}(t), \quad 3 \leq j \leq m-6 \end{split}$$

$$\begin{split} N_{m-5,2}(t) &= \left[\frac{(t-t_{m-5})^2}{(t_{m-4}-t_{m-5})(t_{m-3}-t_{m-5})} \right] N_{m-5,0}(t) + \left[\frac{(t-t_{m-5})(t_{m-3}-t)}{(t_{m-3}-t_{m-5})(t_{m-3}-t_{m-4})} + \cdots \right. \\ &\left. \frac{(t-t_{m-4})(t_{m-2}-t)}{(t_{m-2}-t_{m-4})(t_{m-3}-t_{m-4})} \right] N_{m-4,0}(t), \end{split}$$

$$N_{m-4,2}(t) = \frac{(t-t_{m-4})^2}{(t_{m-2}-t_{m-4})(t_{m-3}-t_{m-4})} N_{m-4,0}(t).$$

$$d = 3$$

$$N_{0,3}(t) = \frac{(t_4 - t)^3}{(t_4 - t_3)(t_4 - t_2)(t_4 - t_1)} N_{3,0}(t),$$

$$N_{1,3}(t) = \left[\frac{(t-t_1)(t_4-t)^2}{(t_4-t_3)(t_4-t_2)(t_4-t_1)} + \frac{(t_5-t)(t-t_2)(t_4-t)}{(t_5-t_2)(t_4-t_2)(t_4-t_3)} + \cdots \right]$$

$$\frac{(t_5-t)^2(t-t_3)}{(t_5-t_2)(t_4-t_3)(t_5-t_3)} \left] N_{3,0}(t) + \frac{(t_5-t)^3}{(t_5-t_2)(t_5-t_3)(t_5-t_4)} N_{4,0}(t), \right.$$

$$\begin{split} N_{2,3}(t) &= \left[\frac{(t-t_2)^2(t_4-t)}{(t_5-t_2)(t_4-t_2)(t_4-t_3)} + \frac{(t_5-t)(t-t_2)(t-t_3)}{(t_5-t_2)(t_5-t_3)(t_4-t_3)} + \cdots \right. \\ &\left. \frac{(t_6-t)(t-t_3)^2}{(t_6-t_3)(t_5-t_3)(t_4-t_3)} \right] N_{3,0}(t) + \left[\frac{(t-t_2)(t_5-t)^2}{(t_5-t_2)(t_5-t_3)(t_5-t_4)} + \cdots \right. \\ &\left. \frac{(t_6-t)(t-t_3)(t_5-t)}{(t_6-t_3)(t_5-t_3)(t_5-t_4)} + \frac{(t-t_4)(t_6-t)^2}{(t_6-t_3)(t_6-t_4)(t_5-t_4)} \right] N_{4,0}(t) + \cdots \\ &\left. \frac{(t_6-t)^3}{(t_6-t_3)(t_6-t_4)(t_6-t_5)} N_{5,0}(t), \right. \end{split}$$

$$\begin{split} N_{j,3}(t) &= \frac{(t-t_j)^3}{(t_{j+3}-t_j)(t_{j+2}-t_j)(t_{j+1}-t_j)} N_{j,0}(t) + \left[\frac{(t-t_j)^2(t_{j+2}-t)}{(t_{j+3}-t_j)(t_{j+2}-t_{j+1})} + \cdots \right. \\ & \frac{(t-t_j)(t_{j+3}-t)(t-t_{j+1})}{(t_{j+3}-t_j)(t_{j+3}-t_{j+1})(t_{j+2}-t_{j+1})} + \cdots \\ & \frac{(t-t_{j+1})^2(t_{j+4}-t)}{(t_{j+4}-t_{j+1})(t_{j+2}-t_{j+1})(t_{j+3}-t_{j+1})} \right] N_{j+1,0}(t) + \cdots \\ & \left[\frac{(t-t_j)(t_{j+3}-t)^2}{(t_{j+3}-t_j)(t_{j+3}-t_{j+1})(t_{j+3}-t_{j+2})} + \cdots \right. \\ & \frac{(t_{j+4}-t)(t-t_{j+1})(t_{j+3}-t)}{(t_{j+4}-t_{j+1})(t_{j+3}-t_{j+2})} + \cdots \\ & \frac{(t-t_{j+2})(t_{j+4}-t)^2}{(t_{j+4}-t_{j+1})(t_{j+4}-t_{j+2})(t_{j+3}-t_{j+2})} \right] N_{j+2,0}(t) + \cdots \\ & \frac{(t_{j+4}-t)^3}{(t_{j+4}-t_{j+1})(t_{j+4}-t_{j+2})(t_{j+4}-t_{j+3})} N_{j+3,0}(t), \quad 3 \leq j \leq m-7 \end{split}$$

$$\begin{split} N_{m-6,3}(t) &= \frac{(t-t_{m-6})^3}{(t_{m-3}-t_{m-6})(t_{m-4}-t_{m-6})(t_{m-5}-t_{m-6})} N_{m-6,0}(t) + \cdots \\ &\left[\frac{(t-t_{m-6})^2(t_{m-4}-t)}{(t_{m-3}-t_{m-6})(t_{m-4}-t_{m-6})(t_{m-4}-t_{m-5})} + \cdots \right. \\ &\left. \frac{(t-t_{m-5})(t-t_{m-6})(t_{m-3}-t)}{(t_{m-3}-t_{m-5})(t_{m-3}-t_{m-6})(t_{m-4}-t_{m-5})} + \cdots \right. \\ &\left. \frac{(t_{m-2}-t)(t-t_{m-5})^2}{(t_{m-2}-t_{m-5})(t_{m-3}-t_{m-5})(t_{m-4}-t_{m-5})} \right] N_{m-5,0}(t) + \cdots \\ &\left[\frac{(t-t_{m-6})(t_{m-3}-t)^2}{(t_{m-3}-t_{m-4})(t_{m-3}-t_{m-5})(t_{m-3}-t_{m-6})} + \cdots \right. \\ &\left. \frac{(t_{m-2}-t)(t-t_{m-5})(t_{m-3}-t)}{(t_{m-2}-t_{m-5})(t_{m-3}-t_{m-4})} + \cdots \right. \\ &\left. \frac{(t-t_{m-4})(t_{m-2}-t)^2}{(t_{m-2}-t_{m-4})(t_{m-2}-t_{m-5})(t_{m-3}-t_{m-4})} \right] N_{m-4,0}(t), \end{split}$$

$$\begin{split} N_{m-5,3}(t) &= \frac{(t-t_{m-5})^3}{(t_{m-2}-t_{m-5})(t_{m-3}-t_{m-5})(t_{m-4}-t_{m-5})} N_{m-5,0}(t) + \cdots \\ &\left[\frac{(t-t_{m-5})^2(t_{m-3}-t)}{(t_{m-2}-t_{m-5})(t_{m-3}-t_{m-5})(t_{m-3}-t_{m-4})} + \cdots \right. \end{split}$$

$$\begin{split} \frac{(t-t_{m-5})(t-t_{m-4})(t_{m-2}-t)}{(t_{m-2}-t_{m-5})(t_{m-2}-t_{m-4})(t_{m-3}-t_{m-4})} + \cdots \\ \frac{(t_{m-1}-t)(t-t_{m-4})^2}{(t_{m-1}-t_{m-4})(t_{m-2}-t_{m-4})(t_{m-3}-t_{m-4})} \bigg] N_{m-4,0}(t), \\ N_{m-4,3}(t) &= \frac{(t-t_{m-4})^3}{(t_{m-1}-t_{m-4})(t_{m-2}-t_{m-4})(t_{m-3}-t_{m-4})} N_{m-4,0}(t). \end{split}$$

are the required cubic basis functions on non-uniform knots.

To find unknown control points:

The corner points Q_k divides the boundary into segments and represents the boundary data points. The starting and end control points are set equal to the first and last boundary data point: $Q_0 = S(0) = P_0$, $Q_m = S(1) = P_m$. For remaining control points, cubic basis functions are used with knots and make it equal to the corresponding data point. In matrix form, it can be written as:

$$NP = R$$

where N is matrix of form

$$N = \begin{bmatrix} N_{1,3}(t_1) & \cdots & N_{n-1,3}(t_1) \\ \vdots & \ddots & \vdots \\ N_{1,3}(t_{m-1}) \cdots & N_{n-1,3}(t_{m-1}) \end{bmatrix}$$

R is a vector of data points

$$R = \begin{bmatrix} Q_1 \\ \vdots \\ Q_{n-1} \end{bmatrix}$$

and P a control points vector

$$P = \begin{bmatrix} P_1 \\ \vdots \\ P_{n-1} \end{bmatrix}$$

2.3. Effect of weights

The NURBS curves have distinct advantages over B spline curves, like B-spline curves are approximating curves and it do not pass through the first and last control points whereas NURBS curves are interpolating curves and pass through first and last control points. The B-spline curves works well if the knots are uniformly spaced while NURBS curves work equally good for any type of knots. The B-spline curves can be changed or altered by changing the position of control points while NURBS curves can be changed by changing the position of knot points and weights as shown in Fig. 3. The NURBS curves are locally control as shown in Fig. 3. In this figure by changing the value of weight w_1 only first two segments $P_1(t)$ and $P_2(t)$ will change third segment $P_3(t)$ will remain unchanged.

With the increase of w_1 value the curve will move toward P_1 control points. Fig. 4 shows the effect of weight w_2 . By changing the value of w_2 all the segments will be effected as the control points will be used in constructing all the segments and the curve moves toward the P_2 control points by increasing the value of w_2 . Similarly Fig. 5 shows the effect of w_4 .

In [23] the authors have constructed the frontal bone fractured part using C^1 rational Ball curves with tangents at end points. The tangent vectors work as intermediate control points. This method works well for small fractured part and gives the tight curve for large fractured parts. If the fractured part break into segments then this gives the good result but computational cost become very high. It is not easy to evaluate intermediate control point and is tough to handle the control points and free shape parameters for multiple segments especially for non mathematicians. This work has overcome all these problems by introducing the proposed method which is more efficient, works well for both small as well as large fractured parts. The input for this method is just knot points and weights. Using this method, fractured part can be divided into segments by the user until the result is satisfied.

2.4. Boundary extraction and corner detection

First step to construct the multiple bones fracture is to get the boundary of each CT scan image. Mathematical morphology defined in [24] is used to obtain the boundary of each CT scan image which is defined as $\beta(A) = A - (A\Theta B)$ where A represents the set of all black pixels, 3×3 structuring element is represented by B and the boundary set of A is represented by $\beta(A)$. — and Θ represent difference and erosion operator, respectively. To divide the boundary in smaller segments we use the corner points. Sarfarz et al. method [25] is used to find the corner points.

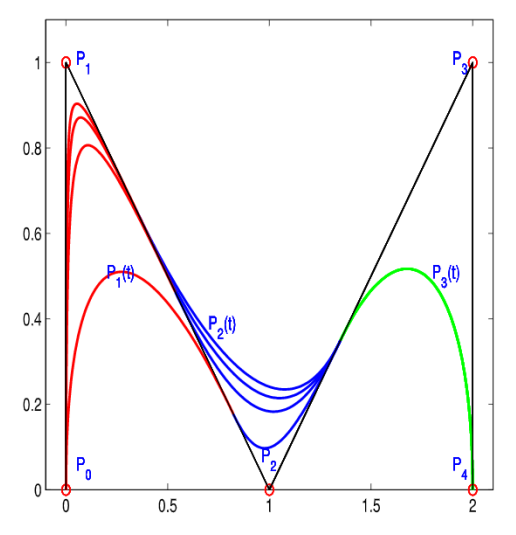


Fig. 3. Effect of weight w_1 .

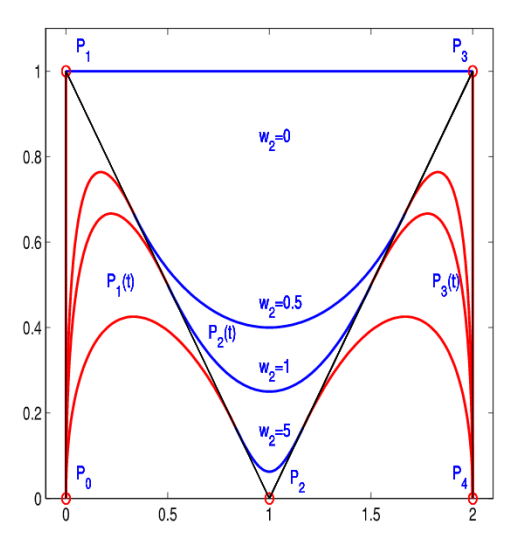


Fig. 4. Effect of weight w_2 .

2.5. Chord length parameterization

Chord length parameterization has been used to find the values of knot vector t_i related to knot points D_i , where D_i represent the knot points of segments,

$$\begin{cases} t_0 = 0, \\ t_k = \frac{\sum_{i=1}^k |D_i - D_{i+1}|}{\sum_{i=1}^n |D_i - D_{i+1}|} & 1 \le k \le n - 1, \\ t_n = 1. \end{cases}$$
(6)

where t_i are in normalized form and varies from 0 to 1.

2.6. Curves to DICOM format

After constructing the fractured part boundary curves of each CT scan image using NURBS curves, the next step is to construct the fractured part into a DICOM format using the method defined in [23]. For this, we take the corner points of both constructed curves and then join the initial and final points by using the following linear form as shown in the second image of Fig. 6:

$$C_i = (1 - t)A_i^* + tB_i^*, i = 0, 1.$$

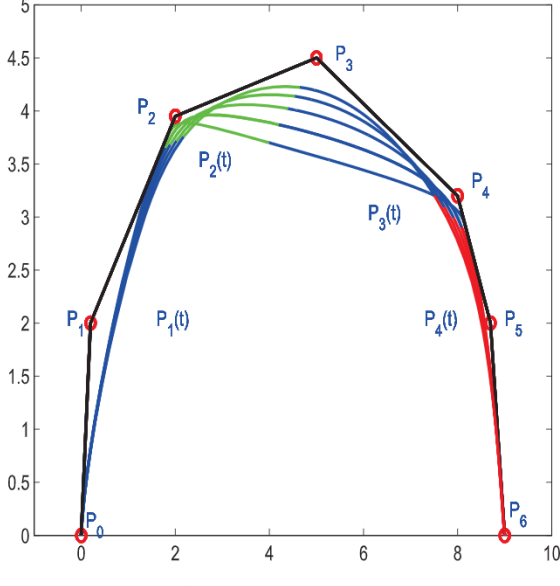


Fig. 5. Effect of weight w_4 .

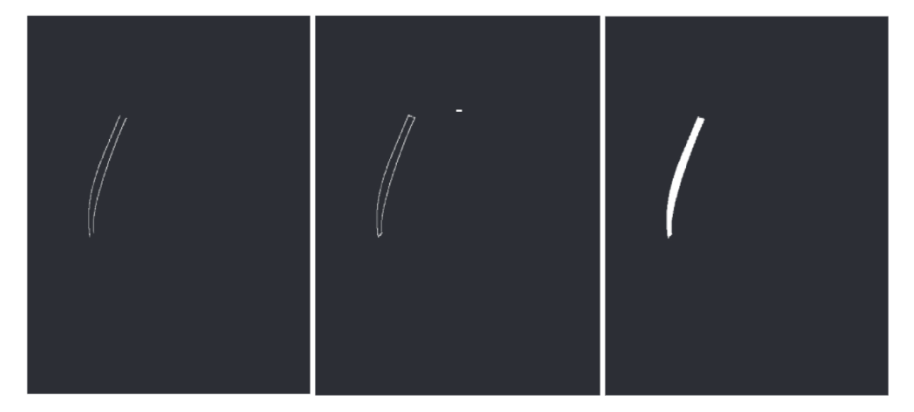


Fig. 6. Curve to DICOM format.

where A_i^* and B_i^* are terminating points of curves, and t varies from 0 to 1. Next step is to take a black image (all zero values) of the same size as the original DICOM image slices Fig. 6(a). The fitted NURBS curves are then converted into white form by equaling this data to 1 as shown in the first image of Fig. 6. MATLAB command imfill is used to fill the area bounded by the fitted curves as shown in the third image of Fig. 6. Software ezDICOM is used to read the constructed DICOM image. Also the constructed images have the same DICOM info as the original CT scan DICOM images have.

3. Multiple bones fracture reconstruction

In this section proposed algorithm, case study of real patient with multiple bones fracture and validity of proposed method are explained.

3.1. Proposed algorithm

This section illustrates the algorithm for multiple bones fracture reconstruction

Input: CT scan image in DICOM format

Output: Constructed fractured part in DICOM format

- 1. Boundary extraction.
- 2. Corner detection in order to convert boundary into segments.
- 3. Estimation of knot values using chord length method.
- 4. Curve fitting using NURBS curves.

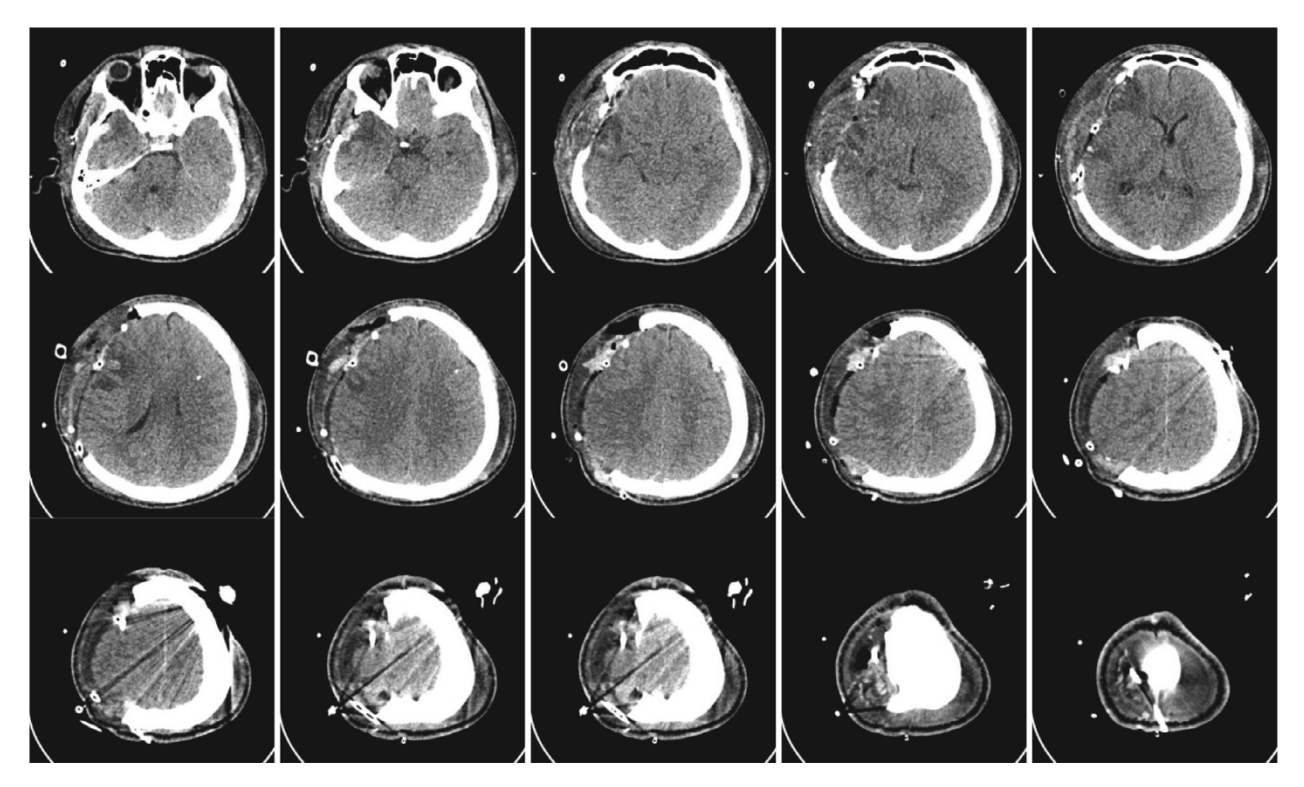


Fig. 7. CT scan images of patient with multiple bones fracture.

Table 1 Errors and weights for Fig. 8(e).

Segments	1	2	3	4	5	6	7
Errors	1.14e-04	3.04e-04	2.4e-04	3.02e-03	5.05e-05	2.2e-04	0.51e-03
Weights	1.2	1.5	0.9	0.89	1.05	2.04	0.5
Time using NURBS	0.04	0.03	0.041	0.044	0.019	0.031	0.036
Time using RCB	0.09	0.084	0.085	0.092	0.087	0.079	0.08
Segments	8	9	10	11	12	13	_
Errors	2.9e - 03	1.3e-02	4.51e-04	2.5e-06	3.7e-03	2.3e-05	_
Weights	1.2	2.5	2.04	1.02	0.5	0.8	-
Time using NURBS	0.028	0.034	0.05	0.048	0.038	0.05	_
Time using RCB	0.070	0.09	0.085	0.086	0.0743	0.09	-

- 5. Construction of multiple bones fractured part boundary curves for each image.
- 6. Construction of multiple bones fracture in DICOM format.

3.2. Case study: reconstruction of multiple bones fracture

This section illustrates the reconstruction of multiple bones fractures using NURBS curves. For this 2D CT scan data in DICOM format are given as shown in Fig. 7. Before constructing the fracture the applicability of proposed method has been tested by reconstructing the complete CT contour (non fractured CT scan contour) as shown in Fig. 8. In this figure part (a) is the original non-fractured CT scan contour, (b) is the outer boundary of bone obtained by using mathematical morphology. Initially we select four points on boundary as a corner points. These corner points divides the boundary into segments which are helpful in reconstructing. The corner points are also used to find the control points and to obtain the knots.

The reconstructed boundary curve did not overlap the original boundary as shown in Fig. 8(a). To get the good result corner points are increased to eight as shown in Fig. 8(d) which gives the better result as before but still the error in some segments is very big. To get the acceptable error, some segments are divided in order to increase the corner points as shown in Fig. 8(e). In this figure red curve is reconstructed boundary curve and black is original boundary. The red curve overlap the black and gives very small error, which shows the applicability and validity of proposed method. Table 1 shows the errors and weights used for the reconstruction of boundary curves. It also shows the computational cost of each segment. Table 2 shows the effect knots values for Fig. 8(c)–(e).

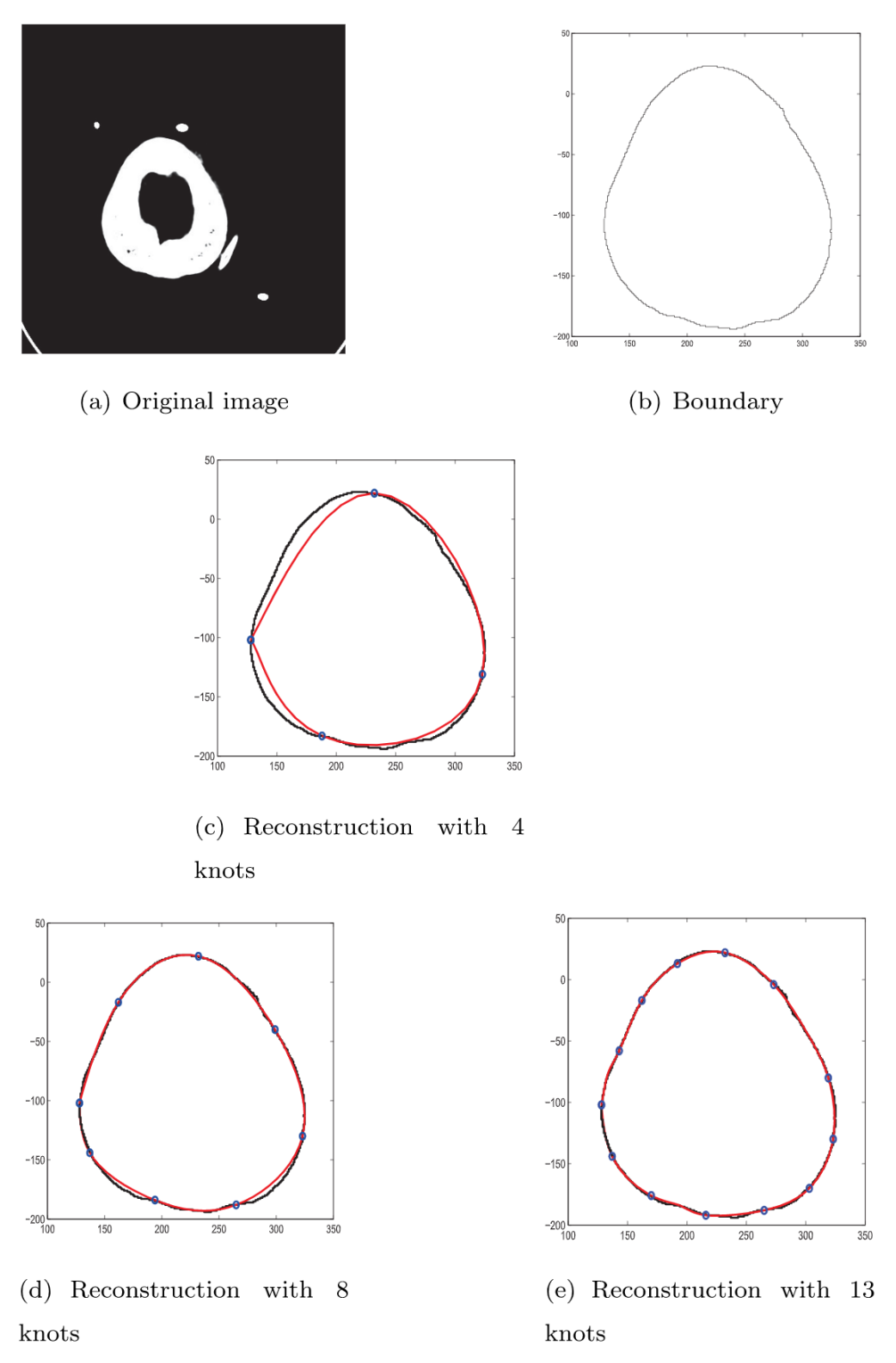
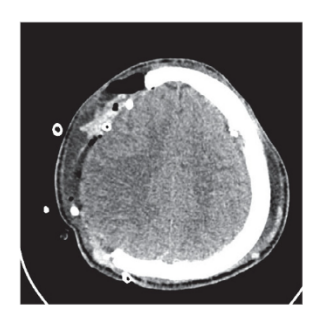
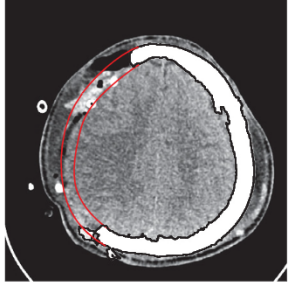


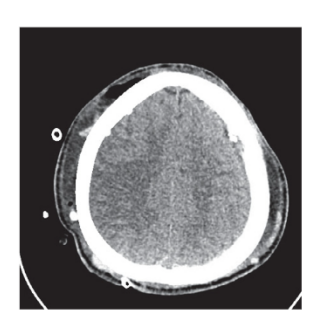
Fig. 8. Reconstruction of complete CT scan contour using NURBS curves.

Table 2 Knots for Fig. 8.

Fig. 8(c)	0	0	0	0	0.3340	0.7014	1	1	1	1
Fig. 8(d)	0	0	0	0	0.1581	0.2966	0.4543	0.6152	0.7569	0.8797
Fig. 8(d)	1	1	1	1	-	-	-	-	-	_
Fig. 8(e)	0	0	0	0	0.0784	0.1545	0.2260	0.2952	0.3770	0.5267
Fig. 8(e)	0.6113	0.6867	0.7575	0.8404	0.9225	1	1	1	1	-







(a) Original image

curves reconstruction

(b) Fractured part boundary (c) Reconstruction of fracture part into DICOM format

Fig. 9. Fractured part reconstruction of slice 154.

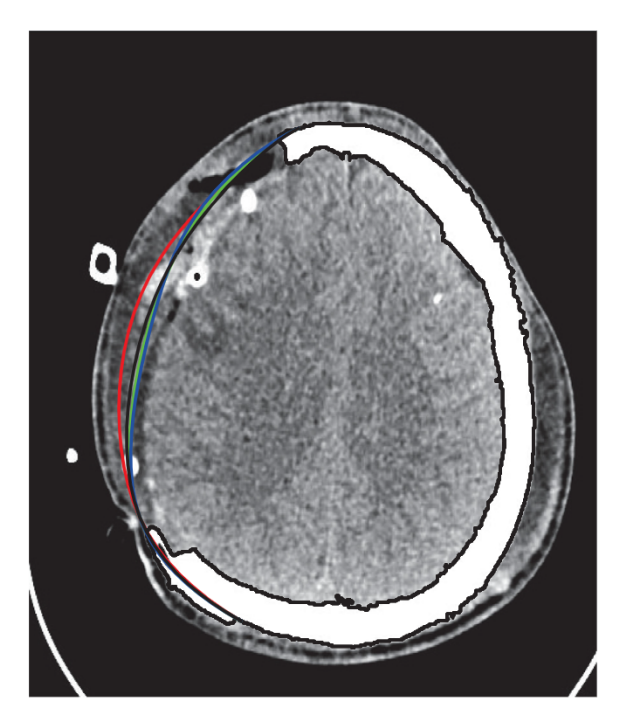


Fig. 10. Effect of weights on fractured part boundary curve.

After checking the applicability and validity of proposed method we employed the proposed method for the construction of fractured part. The construction of fractured part started by reconstructing the inner and outer boundary curves of each CT scan slice as shown in Fig. 9. In this figure part (a) is the original CT scan image and (b) represents the reconstructed boundary curves for fractured part. The input for the construction of boundary curves are the knot values. Using these knot values first we find the knots for cubic basis and then using these knot values we optimized the unknown control points. The weights were optimized using the genetic algorithm. The reconstructed boundary curves can be changed and/or adjusted by changing the weights. The effect of weight on the boundary curves can be seen in Fig. 10. In this figure the

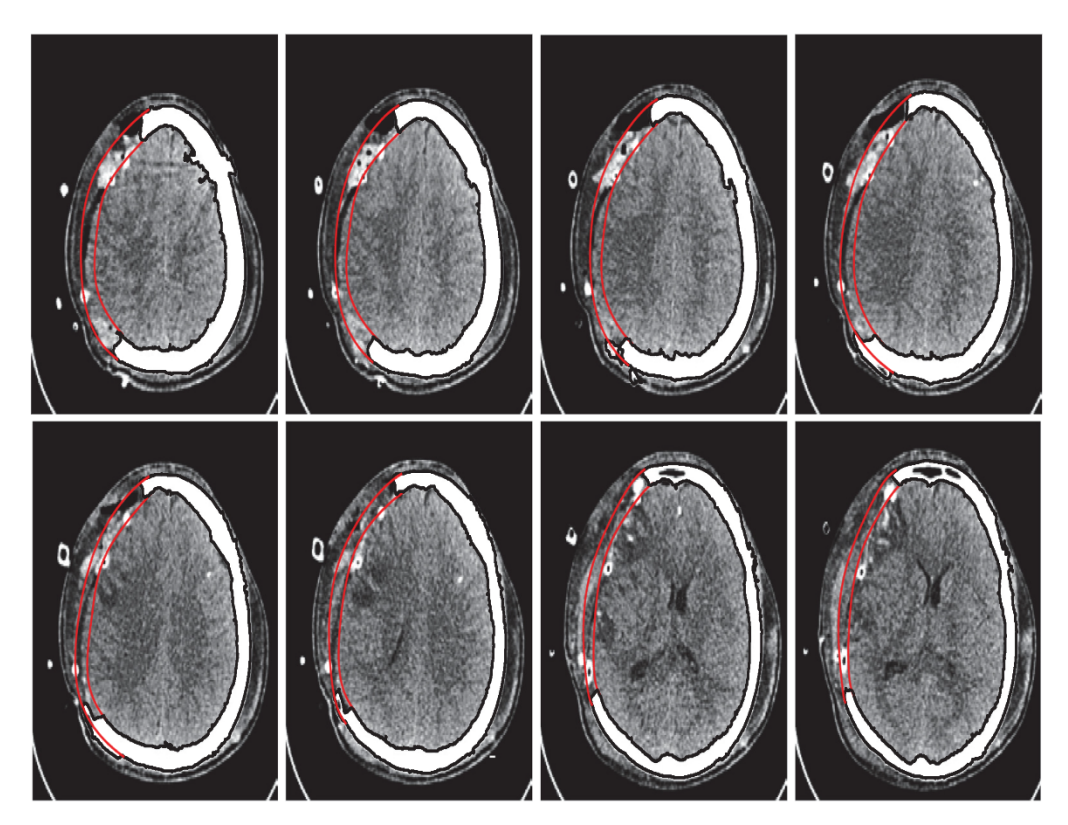


Fig. 11. Reconstructed boundary curves for different CT scan contours.

boundary curve moves outward by increasing the value of w_1 and w_2 . Once we get the desired boundary curves, then we construct the fractured part into DICOM format as shown in Fig. 9(c). The reconstructed boundary curves for different CT scan slices are shown in Fig. 11. The fractured part into DICOM form for different CT scan slices are shown in Fig. 12.

The thickness of skull bone varies from position to position and slice to slice as shown in Fig. 13. In this figure there are three images of same patient with different position having different thickness. The thickness of bone also varies within an image as shown in Fig. 14. Using the proposed method there is no need to take the average thickness of bone and we can attain the required thickness as shown in Fig. 14.

3.3. Validity of proposed method

The proposed method has been validated quantitatively as in Fig. 8(e) and Table 2. The proposed method has also been validated by assuming the parietal bone of non fractured CT scan slice to be fractured. Using the proposed method, we reconstructed those fractured parts and compared with the original as shown in Figs. 15 and 16. In Fig. 15(a) it is the original image and part (b) is the image with the self fractured part. The part (c) represents the reconstructed boundary curves of fractured part using proposed method. Using the reconstructed boundary curves the fractured part has been constructed into DICOM format as shown in Fig. 16. In this figure part (b) is the reconstructed part into DICOM format. Part (c) is the combined image of part (a) and (b). By analyzing part (a) and (c) we see that they look same thus validating our proposed method. Similarly, self supposed fracture of parietal bone on right hand side has been constructed as shown in Figs. 17 and 18.

4. Conclusion

In this article NURBS curves have been used to reconstruct the multiple bones defect of real patient. The reconstruction of the craniofacial defects through this proposed method is based on 2D CT scan DICOM data and is independent of any reference contours or mirror imaging of skull bone and thus, this is user friendly method for neurosurgeons and physicians. The method has been validated qualitatively and quantitatively by real time DICOM data. Using the proposed method, there is no need to take the average thickness as the required thickness can be obtained. The constructed cranial implant is custom made for each patient.

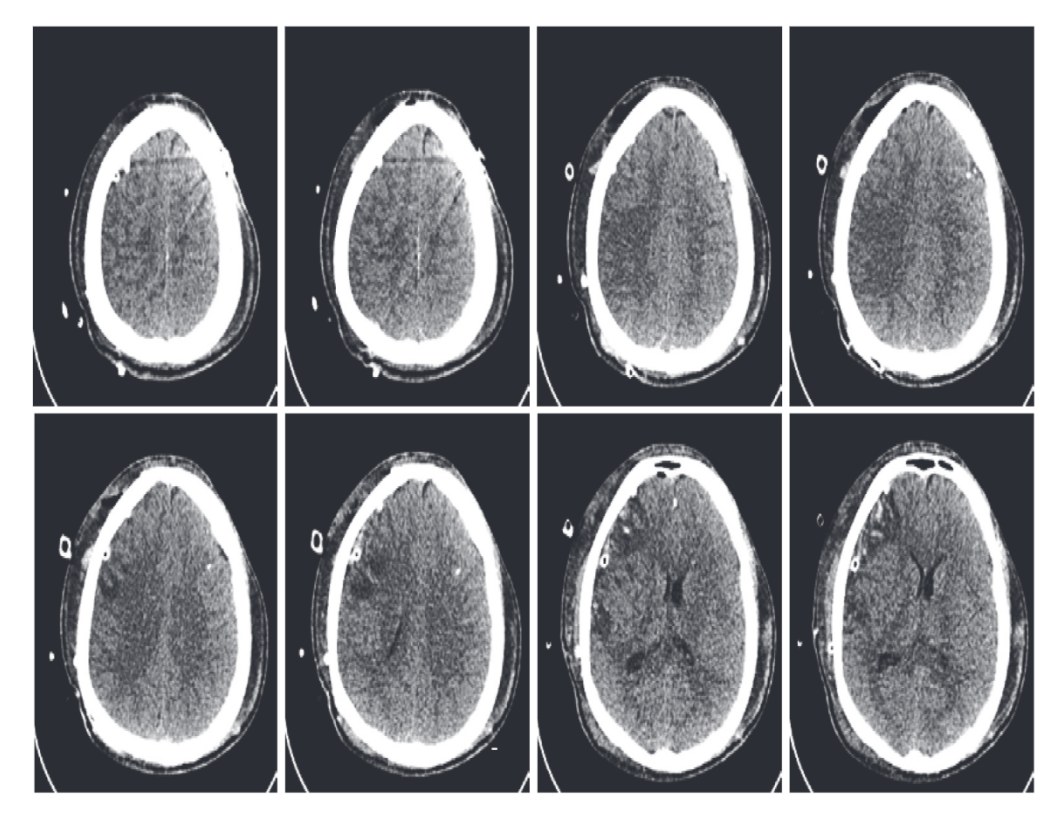


Fig. 12. Fractured part reconstruction for different CT scan contours.

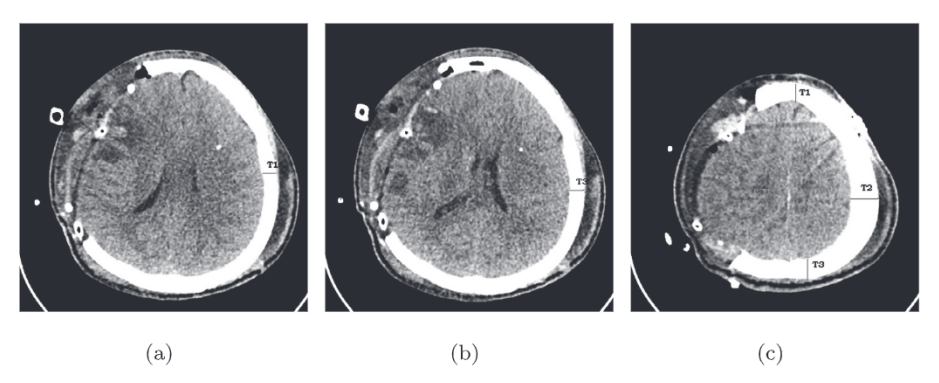


Fig. 13. Thickness of different CT scan images.

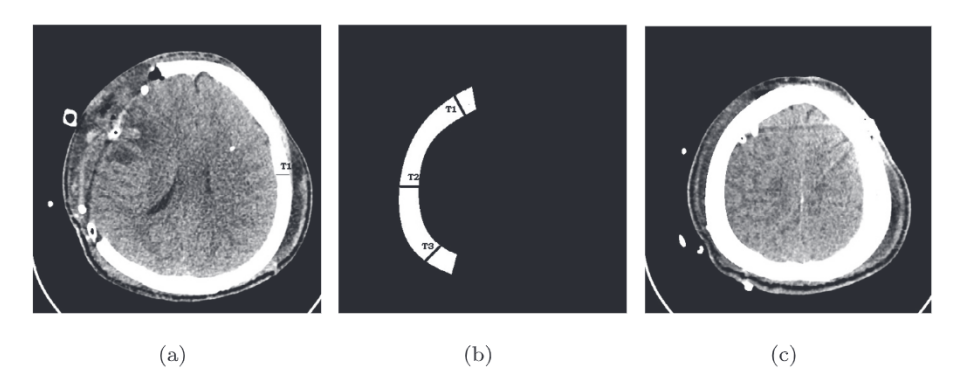


Fig. 14. Thickness of a CT scan image from different positions.

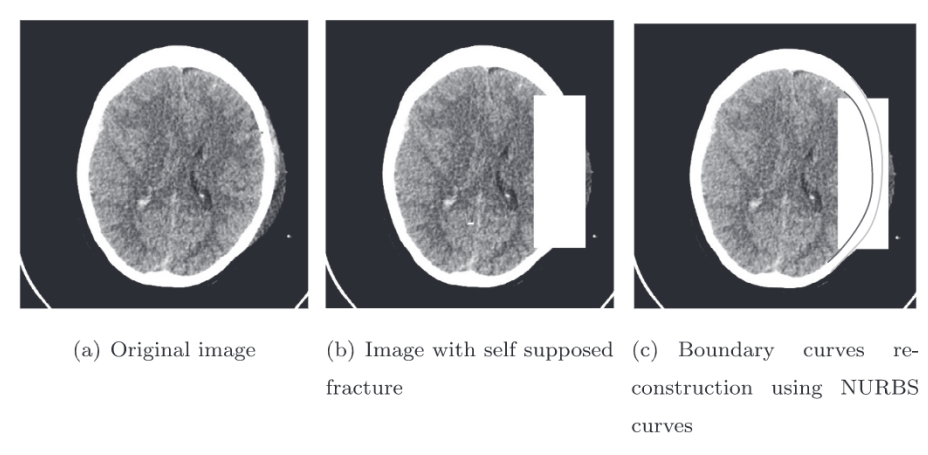


Fig. 15. Reconstructed boundary curves.

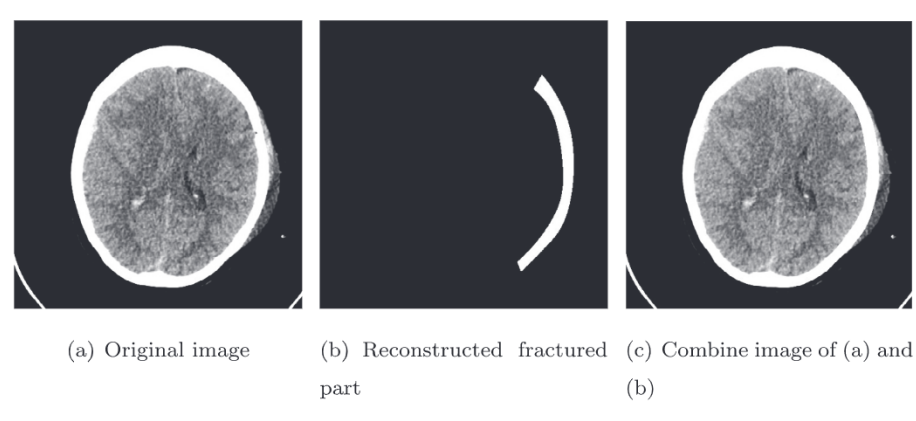


Fig. 16. Self supposed fractured part reconstruction.

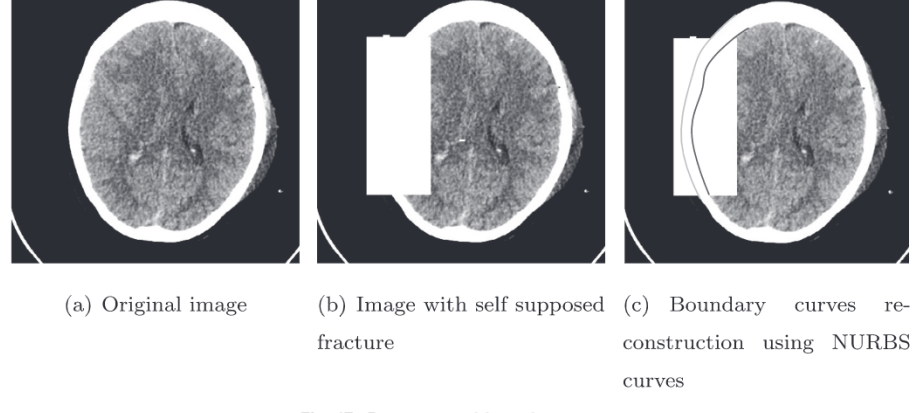


Fig. 17. Reconstructed boundary curves.

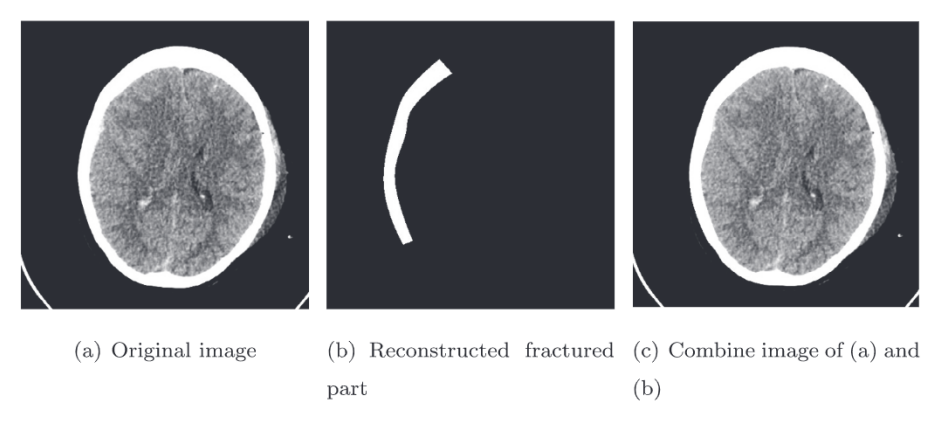


Fig. 18. Self supposed fractured part reconstruction.

Acknowledgments

The authors would like to extend their gratitude to the Ministry of Education of Malaysia and Universiti Sains Malaysia for supporting this work under its USM Research University Grant, Account no. 1001/PPSG/852004.

References

- [1] M.Y. Lee, C.C. Chang, C.C. Lin, L.J. Lo, Y.R. Chen, Custom implant design for patients with cranial defects, IEEE Eng. Med. Biol. Mag. 21 (2) (2002) 38–44.
- [2] A. Mller, K.G. Krishnan, E. Uhl, G. Mast, The application of rapid prototyping techniques in cranial reconstruction and preoperative planning in neuro-surgery, J. Craniofac. Surg. 14 (2003) 899–914.
- [3] V. Sauret, A.D. Linney, R. Richards, Computer assisted surgery: the use of digital images in enabling computerized design and manufacture of titanium implants, Imaging 14 (2002) 464–471.
- [4] W. Shui, et al., 3D craniofacial reconstruction using reference skull-face database, in: Proceedings of the 25th International Conference of Image and Vision Computing New Zealand (IVCNZ), IEEE, 2010.
- [5] T.J.R. Hughes, J.A. Cottrell, Y. Bazilevs, Isogeometric analysis: CAD, finite elements, NURBS, exact geometry and mesh refinement, Comput. Methods Appl. Mech. Eng. 194 (39) (2005) 4135–4195.
- [6] N. Nguyen-Thanh, et al., Isogeometric analysis using polynomial splines over hierarchical T-meshes for two-dimensional elastic solids, Comput. Methods Appl. Mech. Eng. 200 (21) (2011) 1892–1908.
- [7] N. Nguyen-Thanh, et al., Rotation free isogeometric thin shell analysis using PHT-splines, Comput. Methods Appl. Mech. Eng. 200 (47) (2011) 3410–3424.
- [8] H. Nguyen-Xuan, T. Hoang, V.P. Nguyen, An isogeometric analysis for elliptic homogenization problems, Comput. Math. Appl. 67 (9) (2014) 1722-1741.
- [9] S. Yin, et al., Buckling and vibration extended isogeometric analysis of imperfect graded Reissner-Mindlin plates with internal defects using NURBS and level sets, Comput, Struct. 177 (2016) 23–38.
- [10] J.C. Carr, W.R. Fright, R.K. Beatson, Surface interpolation with radial basis functions for medical imaging, IEEE Trans. Med. Imaging 16 (1) (1997)
- [11] J.C. Carr, R.K. Beatson, J.B. Cherrie, T.J. Mitchell, W.R. Fright, B.C. McCallum, T.R. Evans, Reconstruction and representation of 3d objects with radial basis functions, in: Proceedings of the 28th Annual Conference on Computer Graphics and Interactive Techniques, ACM, 2001, pp. 67–76.
- [12] A.S. Chowdhury, S.M. Bhandarkar, R.W. Robinson, J.C. Yu, Virtual craniofacial reconstruction using computer vision, graph theory and geometric constraints, Pattern Recognit. Lett. 30 (10) (2009) 931–938.
- [13] A. Majeed, A.R. Mt Piah, Z. Ridzuan Yahya, Surface reconstruction from parallel curves with application to parietal bone fracture reconstruction, PLoS One 11 (3) (2016), doi:10.1371/journal.pone.0149921. E0149921.
- [14] T.C. Bui, et al., Extended isogeometric analysis for dynamic fracture in multiphase piezoelectric/piezomagnetic composites, Mech. Mater. 97 (2016) 135–163.
- [15] T. Yu, et al., On the thermal buckling analysis of functionally graded plates with internal defects using extended isogeometric analysis, Compos. Struct. 136 (2016) 684–695.
- [16] T.Q. Bui, Extended isogeometric dynamic and static fracture analysis for cracks in piezoelectric materials using NURBS, Comput. Methods Appl. Mech.
- Eng. 295 (2015) 470–509.
 [17] T. Yu, et al., NURBS-based isogeometric analysis of buckling and free vibration problems for laminated composites plates with complicated cutouts
- using a new simple FSDT theory and level set method, Thin-Walled Struct. 101 (2016) 141–156.
 [18] S.D. Greef, G. Willems, Three-dimensional craniofacial reconstruction in forensic identification. Latest progress and new tendencies in the 21st century, J. Forensic Sci. 50 (1) (2005) 12–17.
- [19] P. Claes, D. Vandermeulen, S.D. Greef, G. Willems, P. Suetens, Craniofacial reconstruction using a combined statistical model of face shape and soft tissue depths. methodology and validation, Forensic Sci. Int. 159 (2007) 147–158.
- [20] P. Tu, R. Book, X. Liu, N. Krahnstoever, C. Adrian, P. Williams, Automatic face recognition from skeletal remains, in: Proceedings of Computer Vision and Pattern Recognition (CVPR'07), 2007, pp. 1–7.
- [21] D. Vandermeulen, P. Claes, D. Loeckx, S.D. Greef, G. Willems, Paul Suetens computerized craniofacial reconstruction using CT-derived implicit surface representations, Forensic Sci. Int. 159 (2006) S164–S174.
- [22] A.D. Bhatt, R.M. Warkhedkar, Reverse engineering of human body: a B-spline based heterogeneous modeling approach, Comput.-Aided Des. Appl. 5 (2008) 194–208.
- [23] A. Majeed, A.R. Mt Piah, R.U. Gobithaasan, Z.R. Yahya, Craniofacial reconstruction using rational cubic ball curves, PLoS One 10 (4) (2015) 303, doi:10. 1371/journal.pone.0122854. e0122854.
- [24] A. Majeed, A.R.M. Piah, Image reconstruction using rational ball interpolant and genetic algorithm, Appl. Math. Sci. 8 (74) (2014) 3683-3692.
- [25] M. Sarfraz, M.R. Asim, A. Masood, A new approach to corner detection, in: Computer Vision and Graphics, Springer-Verlag, New York, 2006, pp. 528–533.